J. Fluid Mech. (1992), *vol.* 235, *pp.* 103–121
Printed in Great Britain

Spectral transfer and bispectra for turbulence with passive scalars

By JACKSON R. HERRING[1] AND OLIVER MÉTAIS[2]

[1] National Center for Atmospheric Research, Boulder, CO 80307, USA

[2] Institut de Mécanique Grenoble, Domaine Universitaire, BP 53X, 38041 Grenoble, France

(Received 7 February 1991 and in revised form 2 July 1991)

We examine the statistical mechanisms by which energy and scalar variance are cascaded to small scales for isotropic, three-dimensional turbulence. Two avenues are explored: (i) the traditional transfer function (defined by the nonlinear cascade that gives the time rate of change of the energy spectrum), and (ii) the bispectrum (the elementary triple-point correlation, averaged over directions perpendicular to three co-linear observation points). Our tools are direct numerical simulations (DNS), and the statistical theory of turbulence, here in the form of the test field model (TFM) (Kraichnan 1971). Comparison of the results indicates a fairly good quantitative agreement between DNS and the TFM at large Prandtl numbers ($Pr \geqslant 0.25$), but substantial disagreement at lower Pr, where the transfer to small scales becomes too small. This disparity we trace to the Markovian aspect of the TFM; the more fundamental direct interaction approximation (DIA) (Kraichnan 1959) compares more favourably to DNS as $Pr \to 0$. For $Pr \sim 1$, we compare DNS and TFM bispectra for velocity and scalar fields in both Fourier and physical space. The physical space representation of bispectra serves as a useful means of discriminating between velocity and scalar transfer.

1. Introduction

Perhaps the simplest measurement of turbulence is a single-point, time record of a velocity component or scalar field, such as temperature $y(t)$. Yet the triple-point correlation of such records, $\mathscr{T}(t_1, t_2, t_3) \equiv \langle y(t_1)\, y(t_2)\, y(t_3)\rangle$, the *bispectrum*, contains essential transfer information. Here, as elsewhere in this paper angle brackets denotes ensemble or, where appropriate, time averaging. Note, in this connection, that at large Reynolds number R_λ, $\mathscr{T}$ may be transformed into spatial information via the Taylor hypothesis $\boldsymbol{r}_t = \boldsymbol{v}_0 t_t$, where $\boldsymbol{v}_0$ is the mean speed of the recording device, and r_t are the corresponding spatial points. Of particular importance are bispectra of the form $\langle \boldsymbol{u}(\boldsymbol{x})\, \boldsymbol{u}(\boldsymbol{x}+\boldsymbol{r}_1)\, \boldsymbol{u}(\boldsymbol{x}+\boldsymbol{r}_2)\rangle \equiv B_{uuu}(r_1, r_2)$ where $\boldsymbol{u}$ is the velocity field, since detailed knowledge of this quantity is equivalent to knowing the derivative skewness, $S_{uuu} \equiv -\langle(\partial u/\partial x)^3\rangle / \langle(\partial u/\partial x)^2\rangle^{\frac{3}{2}} \sim -\partial_{x_1}\partial_{x_2}(\partial_{x_1}+\partial_{x_2}) B_{uuu}(x_1, x_2)$, $x_1 \to x_2$, provided that the denominator entering S_{uuu} is also known. Here it should be noted that x_1, x_2 are co-linear. To draw out the physical significance of the bispectra, note that impinging jets with spreading surfaces imply $S_{uuu} > 0$ (Betchov 1957) and the converse. Earlier comparisons of two-point closure (Herring 1980*a*) with both wind tunnel and atmospheric data (see also Van Atta 1979) indicated that both the scaling law for the velocity bispectrum, and the detailed (r_1, r_2) distribution of B_{uuu} were in reasonable accord with experiments.

We describe here a direct numerical simulation (DNS) study of bispectra and

energy transfer mechanisms for decaying turbulence, including the equivalent transfer processes for scalar fields at a range of Prandtl numbers, Pr, ($8 \geqslant Pr \geqslant 0.0625$). We compare DNS results with simple closure formulae, such as those derived from the test field model (TFM) (Kraichnan 1971; Herring & Kraichnan 1972), and, to a more limited extent, the direct interaction approximation (DIA) (Kraichnan 1959). For a scalar θ, we focus on $B_{\theta\theta u} \equiv \langle \theta(\boldsymbol{x}+\boldsymbol{r}_1)\,\theta(\boldsymbol{x}+\boldsymbol{r}_2)\,u(\boldsymbol{x})\rangle$ (The bispectra $B_{\theta\theta\theta}$ are zero for isotropic turbulence). We note that the same arguments relating the velocity skewness to B_{uuu} may here be made to relate $B_{\theta\theta u}$ to the mixed scalar skewness, $S_{\theta\theta u} \equiv -\langle(\partial\theta/\partial x)^2\partial u/\partial x)\rangle/\langle(\partial\theta/\partial x)^2\rangle\langle(\partial u/\partial x)^2\rangle^{\frac{1}{2}}$.

Early studies comparing the closure to experiments for scalar fields (Newman & Herring 1979; Larchevêque *et al.* 1980; Herring *et al.* 1982) suggested that the closure yields qualitatively satisfactory results for the decay of both velocity and passive scalar variances over a range of Reynolds and Prandtl numbers. More recent DNS and LES studies of energy and scalar transfer are those of Kerr (1985), Lesieur & Rogallo (1989), Lesieur, Métais & Rogallo (1989), and Herring (1990). Kerr's DNS study contained extensive information on the behaviour of the scalar for a range of Pr. Finally, the recent study of Métais & Lesieur (1991) examines the probability distribution function for turbulence with both active and passive scalars.

In the present study, we find generally acceptable agreement with respect to energy and scalar variance transfer between DNS and TFM for large Prandtl numbers ($Pr \geqslant 0.25$), but substantial disagreement for low Pr ($Pr \leqslant 0.25$). The failure of simple heuristic theory at low Pr is anticipated by the DNS study of Kerr (1985), who reported mixed scalar skewness substantially larger than those derived from the theory of Batchelor, Howells & Townsend (1959) (referred to hereafter as BHT). We note that at low Pr, the TFM merges with the BHT theory. However, the results of the present study suggest that much of this discrepancy is attributable to the 'Markovian' characterization of the turbulence, inherent in both the BHT and TFM. This suppresses its (TFM) estimate of transfer to small scales for decaying turbulence at low Pr. The DIA does not make such a Markovian characterization: consequently, at the small Péclet numbers encountered as $Pr \to 0$ it has a more vigorous scalar transfer to small scales and agrees better with DNS.

Chasnov, Canuto & Rogallo (1988) have earlier examined the low Pr regime, and report only small departures from the BHT theory. However, their results were for a stationary velocity field, and much of their findings pertained to velocity fields of near Gaussian statistics. The present study differs from theirs in that it involves decaying scalar turbulence with a dynamically evolving velocity field without forcing. The difficulty with the BHT theory noted here may apply only to the case in which Pr is so small that the Péclet number is also small.

A traditional measure of the cascade of energy (or scalar variance) to small scales is the transfer function $T(k,t)$, defined $\ni (\partial_t + \nu k^2)\,E_{u,\theta}(k) = T_{u,\theta}(k)$, where the index on E denotes the variance spectra in question, and ν represents the viscosity or conductivity coefficient. Contrary to $T(k)$, (which has only one degree of freedom), the bispectra (discussed above) are basically two-dimensional, whether viewed in physical space (x_1, x_2) or in their equivalent Fourier representation (k_1, k_2). As yet, experimental studies have focused on Fourier space representations, perhaps because the tools for describing data in this way are more readily available. But for DNS, it is much easier to construct bispectra in physical space. For closures such as the TFM, the physical space construction of the bispectrum is only slightly more trouble than that of the Fourier representation, the latter is an easier basis for posing homogeneous problems.

The physical interpretation of bispectra is clearer in terms of (x_1, x_2) than (k_1, k_2). Thus, contours of $B_{uuu}(x_1, x_2)$ consist of a six-leaf rose, with alternating leaf-signs encountered on rotating around its origin. The principal positive leaf lies along $x_1 = x_2$. Its basic symmetry is

$$B_{uuu}(x_1, x_2) = B_{uuu}(-x_1, x_2 - x_1), \tag{1.1}$$

$$B_{uuu}(-x_1, -x_2) = -B_{uuu}(x_1, x_2), \tag{1.2}$$

$$B_{uuu}(x_1, x_2) = B_{uuu}(x_2, x_1). \tag{1.3}$$

$B_{\theta\theta u}$ on the other hand has only the symmetry

$$B_{\theta\theta u}(x_1, x_2) = B_{\theta\theta u}(x_2, x_1) \tag{1.4}$$

and

$$B_{\theta\theta u}(-x_1, -x_2) = -B_{\theta\theta u}(x_1, x_2). \tag{1.5}$$

The symmetry (1.1) stems from homogeneity, whereas (1.3) and (1.4) are definitional. Symmetries (1.2) and (1.5) characterize turbulence whose statistics is reflectionally invariant. None of these are concerned with isotropic turbulence. Generally, in DNS (1.2) and (1.5) would be satisfied only approximately. Returning to the discussion of bispectra results, we find that the principle positive leaf of $B_{\theta\theta u}$ is much narrower than that of B_{uuu}. In Fourier space, the higher symmetry of B_{uuu} indicates that its first quadrant specification implies its knowledge in the entire (x_1, x_2) plane. This is not true of $B_{\theta\theta u}$; it is asymmetric with respect to $k_2 \to -k_2$.

2. Theoretical concepts and definitions

We describe here in detail the application of the theory for the scalar field, and defer to the earlier study (Herring 1980*a*) for the velocity field results. To begin, consider the mixed scalar bispectrum:

$$B_{\theta\theta u_i} \equiv \langle u_i(\boldsymbol{x})\, \theta(\boldsymbol{x}+\boldsymbol{r}_1)\, \theta(\boldsymbol{x}+\boldsymbol{r}_2)\rangle, \tag{2.1}$$

where $\boldsymbol{r}_1, \boldsymbol{r}_2$ are collinear with u_i, and angular brackets denote ensemble averages. The Fourier transform of $B_{\theta\theta u_i}$ is

$$B_{\theta\theta u_i}(k_1, p_1) = (2\pi)^{-2} \int_{-\infty}^{\infty} \mathrm{d}r_1\, \mathrm{d}r_2\, B_{\theta\theta u_i}(r_1, r_2) \exp\left(-\mathrm{i}(r_1 k_1 + r_2 p_1)\right), \tag{2.2}$$

where $\boldsymbol{k} = (k_1, k_2, k_3)$. $B_{\theta\theta u_i}(k_1, p_1)$ is related to the Fourier transform of $\theta(\boldsymbol{x}) \equiv \sum_{\boldsymbol{k}} \theta(\boldsymbol{k}) \exp(\mathrm{i}\boldsymbol{k}\cdot\boldsymbol{x})$ by

$$B_{\theta\theta u_i}(k_1, p_1) = \left(\frac{L}{2\pi}\right)^6 \int_{-\infty}^{\infty}\int_{-\infty}^{\infty} \mathrm{d}\boldsymbol{k}_\perp\, \mathrm{d}\boldsymbol{p}_\perp \langle \theta(\boldsymbol{k})\, \theta(\boldsymbol{p})\, u_i(\boldsymbol{q})\rangle, \tag{2.3}$$

where $\boldsymbol{q} = -\boldsymbol{k} - \boldsymbol{p}$, and $\mathrm{d}\boldsymbol{k}_\perp \equiv (\mathrm{d}k_2\, \mathrm{d}k_3)$, etc. L^3 is the normalizing volume. We assume L is sufficiently large so that the approximation

$$\sum \approx (L/2\pi)^3 \int \mathrm{d}\boldsymbol{k} \tag{2.4}$$

applies with impunity. The mixed scalar skewness $S_{\theta\theta u_i}$ is computable from $B_{\theta\theta u_i}$ from

$$S_{\theta\theta u_i} \equiv -\frac{\langle (\partial u/\partial x)\, (\partial\theta/\partial x)^2\rangle}{N_{u\theta\theta}}$$

$$= -\mathrm{i} \int_{-\infty}^{\infty}\int_{-\infty}^{\infty} \frac{\mathrm{d}k_1\, \mathrm{d}p_1\, k_1\, p_1 (k_1 + p_1) B_{u_i\theta\theta}(k_1, p_1)}{N_{u\theta\theta}}, \tag{2.5}$$

where $N_{abc} \equiv (\langle(\partial a/\partial x)^2\rangle \langle(\partial b/\partial x)^2\rangle \langle(\partial c/\partial x)^2\rangle)^{\frac{1}{2}}$. The velocity derivative skewness $S_{uuu} \equiv -\langle(\partial u/\partial x)^3\rangle / \langle(\partial u/\partial x)^2\rangle^{\frac{3}{2}}$ is given by a formula identical to (2.5) except that $\theta \to u$.

We describe next the approximations to the basic dynamic quantities, $\langle u_i(\boldsymbol{q}) u_j(\boldsymbol{k}) u_l(\boldsymbol{p})\rangle$ and $\langle u_i(\boldsymbol{q}) \theta(\boldsymbol{k}) \theta(\boldsymbol{p})\rangle$, via the TFM (Kraichnan 1971; Herring & Kraichnan 1972). The application of this theory to the velocity bispectrum has been investigated earlier (Herring 1980*a*). For subsequent reference, we will sketch the TFM evaluation of triple moments needed to evaluate (2.1) according to the closure, without much by way of rigour. Basically, we follow Kraichnan's (1959) direct interaction approximation (DIA) algorithm treating $[u_i(\boldsymbol{k}), \theta(\boldsymbol{k})]$ as a discrete collection of interacting degrees of freedom, whose multivariate statistics are nearly Gaussian. Correlations in (2.3) between modes $(\boldsymbol{k}, \boldsymbol{p}, \boldsymbol{q})$ are induced through the interactions among this triplet as implied by the equation of motion for $\theta(\boldsymbol{k})$. The latter is

$$\partial_t \theta = \kappa \nabla^2 \theta - \boldsymbol{u} \cdot \nabla \theta \tag{2.6}$$

or, in Fourier representation,

$$\partial_t \theta(\boldsymbol{k}) = -\kappa k^2 \theta(\boldsymbol{k}) - \mathrm{i} p_m u_m(-\boldsymbol{q}) \theta(-\boldsymbol{p}) - \mathrm{i} q_m u_m(-\boldsymbol{p}) \theta(-\boldsymbol{q}) - \mathrm{i} \sum_{\boldsymbol{k}=\boldsymbol{p}'+\boldsymbol{q}'} q'_m u_m(\boldsymbol{p}') \theta(\boldsymbol{q}'). \tag{2.7}$$

In (2.7), we have split from the convolution sum that part explicitly referencing the triplet $\boldsymbol{k}, \boldsymbol{p}, \boldsymbol{q}$ (the second and third terms on the right-hand side). The primes on the last term here indicate the omission of the second two terms, which are explicitly broken out. We then treat $\langle \theta(\boldsymbol{k}) \theta(\boldsymbol{p}) \theta(\boldsymbol{q})\rangle$ as perturbatively small, writing it as $\langle \delta\theta(\boldsymbol{k}) \theta(\boldsymbol{p}) \theta(\boldsymbol{q}) + \theta(\boldsymbol{k}) \delta\theta(\boldsymbol{p}) \theta(\boldsymbol{q}) + \theta(\boldsymbol{k}) \theta(\boldsymbol{p}) \delta\theta(\boldsymbol{q})\rangle$, with $\delta\theta(\boldsymbol{k}, t)$ given by

$$\delta\theta(\boldsymbol{k}, t) \approx -\int_0^t \mathrm{d}s\, g^\theta(\boldsymbol{k}, t, s) \{\mathrm{i} p_m u_m(-\boldsymbol{q}, s) \theta(-\boldsymbol{p}, s) + \mathrm{i} q_m u_m(-\boldsymbol{p}, s) \theta(-\boldsymbol{q}, s)\} + \ldots. \tag{2.8}$$

In (2.8) $g^\theta(\boldsymbol{k}, t, s)$ is the response of mode $\theta(\boldsymbol{k})$ induced by a small perturbative force in which only the interactions of $\theta(\boldsymbol{k})$ with $(\boldsymbol{p}', \boldsymbol{q}')$ that can be represented in terms of an eddy conductivity are included. For what follows, we replace g^θ by its ensemble mean, $G^\theta(\boldsymbol{k}, t, s)$, and parameterize the latter as

$$G^\theta(\boldsymbol{k}, t, s) \approx \exp(-\eta^\theta(k)(t-s)). \tag{2.9}$$

Formulae for $\eta^\theta(k)$ are given in §3. To complete the calculation, we use (2.8) with (2.9) in the perturbative expression and evaluate the resulting fourth-order moments as if Gaussian. The result is

$$\langle u_n(-\boldsymbol{k}-\boldsymbol{p}) \theta(\boldsymbol{k}) \theta(\boldsymbol{p})\rangle = \tfrac{1}{2}\mathrm{i}\{p_n - q_n(\boldsymbol{p}\cdot\boldsymbol{q}/q^2)\} \{U(q)\Theta(p) - U(q)\Theta(k)\}\{\eta^\theta(k) + \eta^\theta(p)) + \eta^s(q)\}^{-1}, \tag{2.10}$$

where

$$U(k) = (L/2\pi)^3 \langle u_i(\boldsymbol{k}) u_i(-\boldsymbol{k})\rangle, \tag{2.11}$$

$$\Theta(k) = (L/2\pi)^3 \langle \theta(\boldsymbol{k}) \theta(-\boldsymbol{k})\rangle. \tag{2.12}$$

In (2.10) $\boldsymbol{q} = -\boldsymbol{k} - \boldsymbol{p}$, and the η are relaxation rates for the velocity and scalar fields. They may be approximated by (Herring *et al.* 1982):

$$\eta^s(k) \approx 0.4 \left\{\int_0^k p^2 E(p)\right\}^{\frac{1}{2}},$$

$$\eta^\theta(k) \approx 2\eta^s(k).$$

We describe the determination of the g-factors in §3. The DIA equivalent to the right-hand side of (2.10) is

$$\tfrac{1}{2}\mathrm{i}\{p_i-(\boldsymbol{p}\cdot\boldsymbol{q})\,q_i/q^2\}\int_0^t \mathrm{d}s\,G^\theta(k,t,s)\,\Theta(p,t,s)\,U(q,t,s)+(p\to q),$$

where $G^\theta(k,t,s)$ is the scalar Green's function. The approximations needed to reduce the DIA expression to (2.10) are clear. Finally, we must perform the $(\mathrm{d}\boldsymbol{p}_\perp\,\mathrm{d}\boldsymbol{q}_\perp)$ integrals in (2.3), for which cylindrical coordinates are convenient. Details are in Herring (1980*a*).

3. Energy and scalar variance transfer: comparisons with numerical simulations at moderate R_λ

We first compare the predictions of the TFM–DIA for energy and scalar variance transfer T_u, T_θ defined as $\ni(\partial_t+2(\nu,\kappa k^2)E_{u,\theta}(k,t)=T_{u,\theta}(k,t))$ to DNS for decaying turbulence with a passive scalar field. To study this, we need equations of evolution for $E_u(k,t)\equiv 2\pi k^2U(k)$, and $E_\theta(k)\equiv 2\pi k^2\Theta(k)$. Using the same approximation used to derive (2.10), these are

$$\{\partial_t+2\nu k^2\}\,U(k,t)=\int_\Delta \mathrm{d}p\,\mathrm{d}q\,B_u(k,p,q)\,U(q)\,\{U(p)-U(k)\}\,D_v(k,p,q), \tag{3.1}$$

$$\{\partial_t+2\kappa k^2\}\,\Theta(k,t)=\int_\Delta \mathrm{d}p\,\mathrm{d}q\,B_\theta(k,p,q)\,U(q)\,\{\Theta(p)-\Theta(k)\}\,D_\theta(k,p,q), \tag{3.2}$$

with
$$B_u(k,p,q)\equiv\pi\sin^2(p,q)\,((p^2-q^2)\,(k^2-q^2)+p^2k^2)\,pq/k^2 \tag{3.3}$$

$$B_\theta\equiv\pi\sin^2(p,q)\,p^3q/k. \tag{3.4}$$

In the TFM, D_v, D_θ satisfy

$$\{\partial_t+\nu(k^2+p^2+q^2)+\eta^s(k)+\eta^s(p)+\eta^s(q)\}\,D_v(k,p,q)=1, \tag{3.5}$$

$$\{\partial_t+\kappa(k^2+p^2)+\nu q^2+g_\theta^2(\eta^c(k)+\eta^c(p))+\tilde{g}_\theta^2\,\eta^s(q)\}\,D_\theta(k,p,q)=1, \tag{3.6}$$

and $\eta^{s,c}(k)$ are
$$\eta^s(k)=\tfrac{1}{2}g^2\int_\Delta \mathrm{d}p\,\mathrm{d}q\,C(k,p,q)\,D_g(k,p,q)\,U(q), \tag{3.7}$$

$$\eta^c(k)=\int_\Delta \mathrm{d}p\,\mathrm{d}q\,C(k,p,q)\,D_g(k,p,q)\,U(q), \tag{3.8}$$

$$\left.\begin{aligned} C(k,p,q)&=\pi kpq(1-y^2)\,(1-z^2),\\ (y,z)&=(\sin(\boldsymbol{k},\boldsymbol{q}),\sin(\boldsymbol{k},\boldsymbol{p})),\end{aligned}\right\} \tag{3.9}$$

$$\{\partial_t+\nu(k^2+p^2+q^2)+\eta^c(k)+\eta^c(p)+\eta^s(q)\}\,D_g(k,p,q)=1. \tag{3.10}$$

As originally proposed (Kraichnan 1971; Herring & Kraichnan 1972), equations (3.5) and (3.6) contain arbitrary scaling factors g and g_θ. Equation (3.6) follows from Kraichnan's (1971) suggestion that the scalar eddy-relaxation rate $\eta^\theta(k)$ be proportional to the relaxation rate $(\eta^c(k))$ of a compressive field convected by $\boldsymbol{u}$. Equation (3.6) has an additional factor $\tilde{g}_\theta$. It is arbitrary if (3.1)–(3.10) are derived via the eddy-damped quasi-normal Markovian (EDQNM) approximation (Larchevêque & Lesieur 1981), but is unity if determined by comparison with DIA. The values of the g are set either by comparison to experiments or by an appeal to more basic theory. Larchevêque & Lesieur (1981), for example, following an abridged

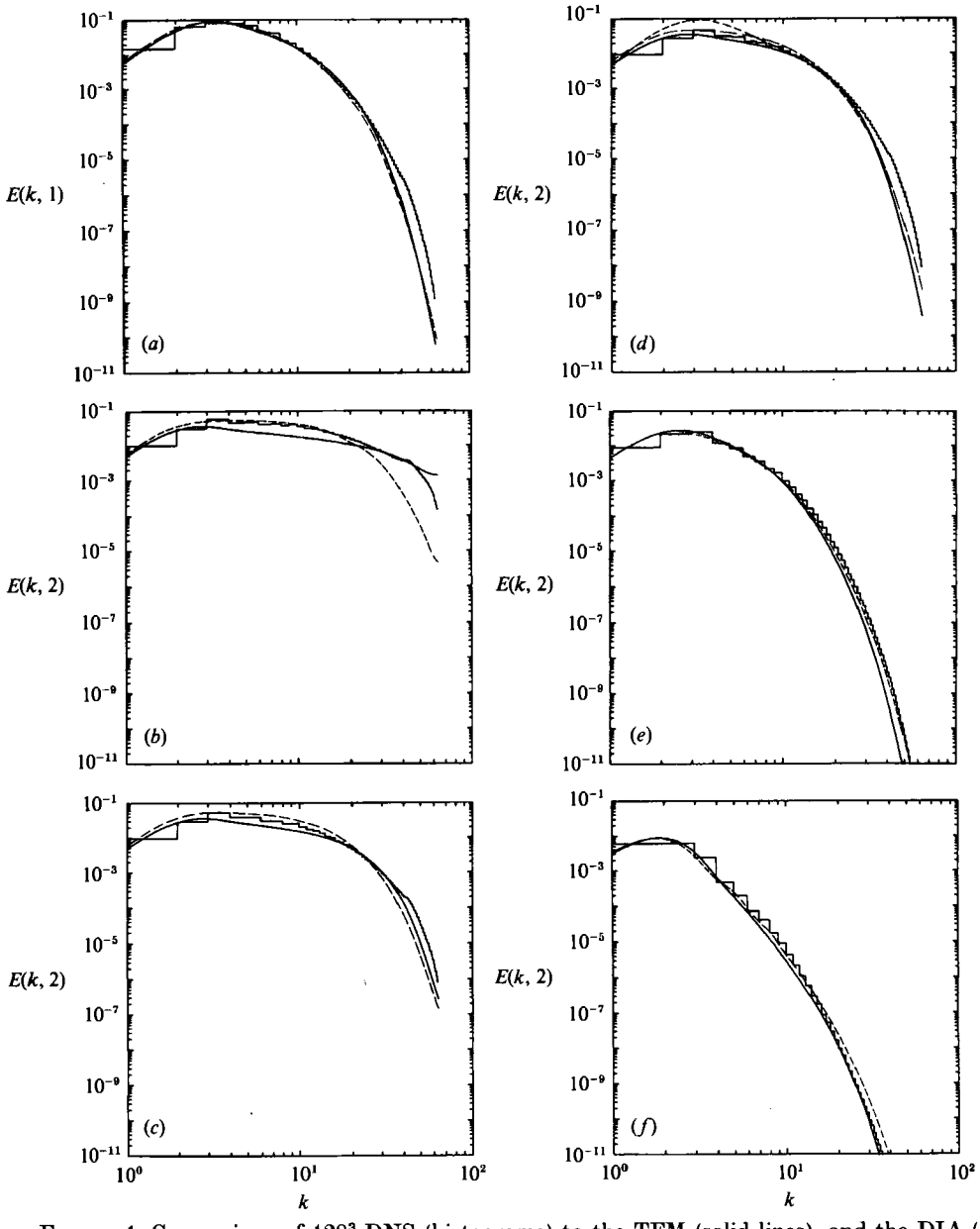

FIGURE 1. Comparison of 128^3 DNS (histograms) to the TFM (solid lines), and the DIA (dashed lines) at $t = 1.0$. (*a*) Energy spectrum, labelled $E(k, 1)$. Scalar spectra (labelled $E(k, 2)$) are given in (*b*, *c*, *d*, *e*, *f*) for $Pr = (8.0, 2.0, 1.0, 0.25, 0.0625)$, respectively. TFM parameters (see (3.6) and (3.7)) are $(g, g_\theta, \tilde{g}_\theta) = (1.16, 0.5, 1.0)$. In (*d*), the long-dashed line is the DIA, while the short-dashed line is TFM with $(g_\theta, \tilde{g}_\theta = 0, 3.61)$.

Lagrangian history (Kraichnan 1964) analogy, proposed $g_\theta = 0$, and $\tilde{g}_\theta = 3.61$. This choice corresponds to no memory loss for the scalar along Lagrangian trajectories ($g_\theta = 0$), and to the condition that at large Reynolds and Péclet numbers, the Corrsin–Oboukhov constant $C_{\rm CO} = 0.67$, ($E_\theta(k) = C_{\rm CO}\,\epsilon_\theta/\epsilon_v^{\frac{2}{3}}\,k^{-\frac{5}{3}}$). Here ϵ_v and ϵ_θ are the dissipation of kinetic energy and scalar variance. Their choice has the additional virtue of predicting a satisfactory value of the Batchelor *et al.* (1959) constant at

large Pr, and of producing analytically tractable forms for certain turbulence quantities (for example, pair dispersion by turbulent motion). Other theoretical proposals to determine (g, g_θ, and $\tilde{g}_\theta$) are based on the requirement that the TFM yield the same results as the DIA (which has no arbitrary constants) for a problem for which the DIA is thought to be accurate. Kraichnan proposed that such a comparison case be thermal equilibrium ($\nu = \kappa = 0$) for the system comprising a band of wavenumber $k_0 - \epsilon \leqslant k \leqslant k_0 + \epsilon, \epsilon \to 0$. An alternative comparison problem is to require the TFM and DIA to agree as $k \to 0$, *provided* the DIA is exponentially parameterized, as in (2.9). The last two alternatives yield nearly the same results for practical purposes: ($g = 1.116$, $g_\theta = 0.5$, and $\tilde{g}_\theta = 1.0$). Identifying the coefficients by a $k \to 0$ comparison of theories is quite similar to the renormalization group computation of Dannevik, Yakhot & Orszag (1987). In any case, in our comparisons with DNS, one preliminary consideration is the optimal choice of g_θ, and $\tilde{g}_\theta$. A more important consideration is to form an assessment of the accuracy, particularly over a range of Pr.

Here the TFM, DIA, and DNS are compared for $R_\lambda \sim 30.0$, and for initial $E_u(k,0), E_\theta(k,0)$ spectra of the form

$$E_u(k) = 16(2/\pi)^{\frac{1}{2}}(u_0^2)\,(k_u^{-5})\,k^4 \exp(-2(k^2/k_u^2)), \tag{3.11a}$$

$$E_\theta(k) = 16(2/\pi)^{\frac{1}{2}}(\theta_0^2)\,(k_\theta^{-5})\,k^4 \exp(-2(k^2/k_\theta^2)). \tag{3.11b}$$

Initial conditions for the DNS $\boldsymbol{u}(\boldsymbol{k},0)$ and $\theta(\boldsymbol{k},0)$ are uncorrelated, Gaussian random numbers as generated by standard pseudo-random number procedure (Kerr 1985), and $k_u = k_\theta = 4.757$. The DNS spectra are (3.11a, b), with ensemble averages interpreted as wave-number, unit-shell averages, i.e.

$$\langle Q(\boldsymbol{k})\rangle(k) \equiv \sum_{k-\frac{1}{2} \leqslant |\boldsymbol{k}| \leqslant k+\frac{1}{2}} Q(\boldsymbol{k}), \quad k = (1,2,\ldots). \tag{3.12}$$

In (3.11) $u_0 = \theta_0 = 1.0$ are the initial r.m.s. values of velocity and the scalar. With a value of viscosity $\nu = 0.01189$, the Taylor microscale Reynolds number, $R_\lambda(t=0) = 35.0$. These choices for u_0 and ν guarantee a well-resolved dissipation range (for both the DNS and TFM) during the course of the run ($t \leqslant 1.0$, where the unit of time is $L/(E_u(0))^{\frac{1}{2}}$, with L the initial integral scale and $E_u(0)$ the initial energy). The peak wavenumber, k_u, is sufficiently large (compared to the DNS low wavenumber cutoff ($k_1 = 1.0$)) that interactions in the neighbourhood of $k \sim 1$ play a negligible role in the higher-k dynamics.

We examine first how faithfully the TFM and DIA track the energy transfer processes for $\boldsymbol{u}$ and θ. We do not record the DIA equivalent of (3.1)–(3.10), for the sake of brevity; they may be found in Newman & Herring (1979). Comparisons are made here for initial spectra (3.11) and for a range of Prandtl numbers: $Pr = 8.0, 2.0, 1.0, 0.25, 0.0625$. The comparisons (figure 1) are at $t = 1.0$. Shown are $E_u(k, t=1)$ (figure 1a), and $E_\theta(k, t=1)$ in figure 1(b–f) for ($Pr = 8.0, 2.0, 1.0, 0.25, 0.0625$), respectively. Figure 2 shows the same comparison for the energy transfer spectra, $T_u(k,t), T_\theta(k,t)$ (recall, $T_{u,\theta}(k) \ni \{\partial_t + 2(\nu,\kappa)k^2\}E_{u,\theta}(k) = T_{u,\theta}$). TFM results are for parameters $g, g_\theta, \tilde{g}_\theta = (1.16, 0.5, 1.0)$ only, except for figure 1(d), where the short-dashed line indicates the choice ($g_\theta, \tilde{g}_\theta = 0, 3.61$) (see (3.6)). The latter corresponds to the EDQNM choice of Larchevêque & Lesieur (1981). DIA results in figures 1 and 2 are indicated by the dashed lines; in figure 1(d), the DIA is the long-dashed line.

Figure 1 suggests that the DIA is more accurate in the energy-containing range but less so than the TFM for the dissipation range. For our purposes, we may take

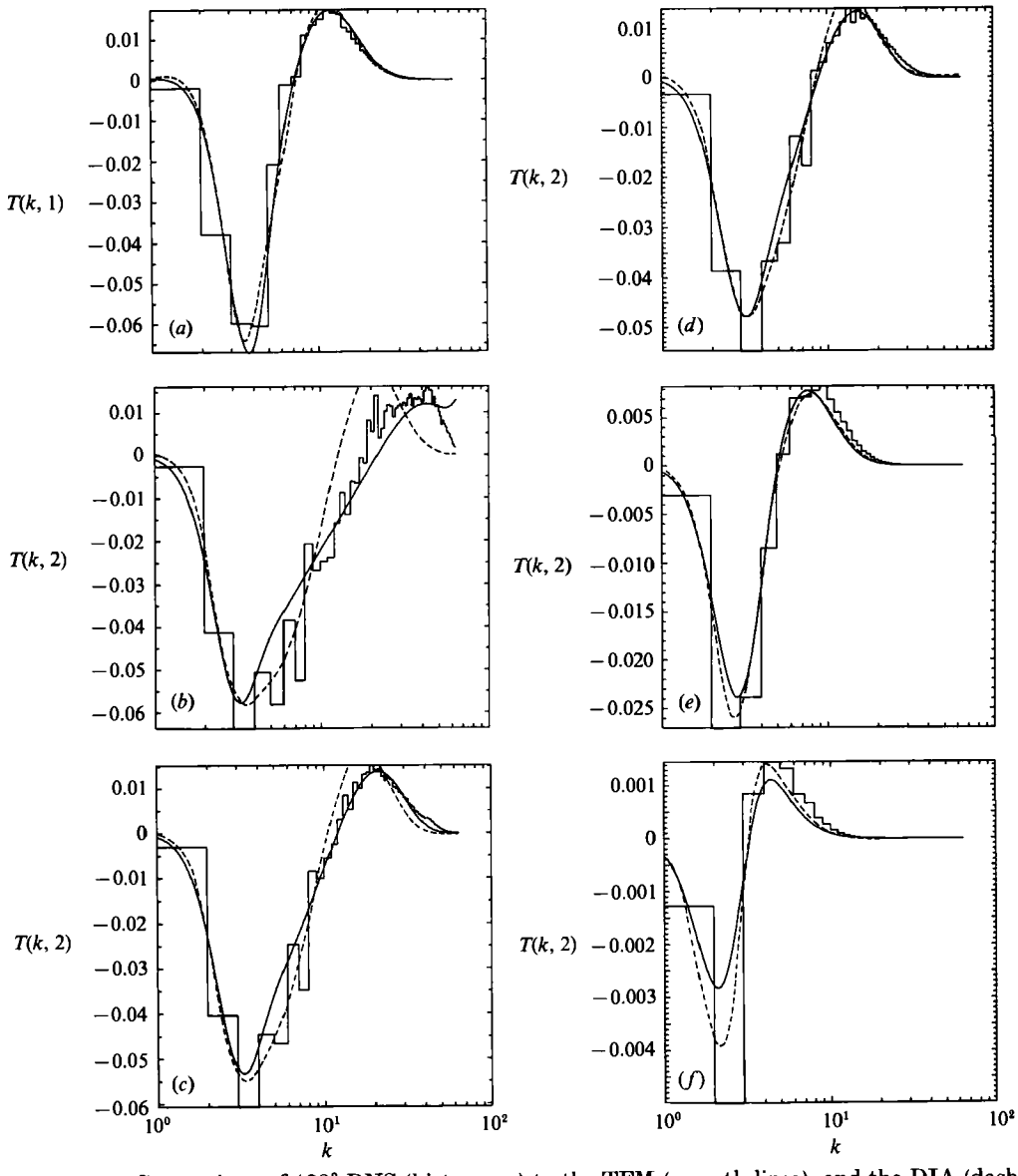

FIGURE 2. Comparison of 128^3 DNS (histogram) to the TFM (smooth lines), and the DIA (dashed lines). (*a*) Energy transfer spectrum $T(k, 1)$. Scalar variance transfer spectra, $T(k, 2)$ are given in (*b, c, d, e, f*) for $Pr = (8.0, 2.0, 1.0, 0.25, 0.0625)$, respectively. The TFM parameters (see (3.6) and (3.7)) are: $(g, g_\theta, \tilde{g}_\theta) = (1.16, 0.5, 1.0)$. $T(k) \ni (\partial_t + 2\nu\kappa^2) E_{u\theta}(k) = T_{u\theta}$.

the 'energy-containing range' as the region in wavenumber where $T(k) < 0$, and the dissipation range as where the converse is so. At the R_λ considered here (~ 20), the inertial range is vestigial, but would occur (at much higher R_λ) where $T(k) \sim 0$. The large DIA errors at large k result from the spurious dependence of its $T_{u,\theta}(k)$ on large-scale sweeping. At lower $Pr(\approx 0.25, 0.0625)$, the DIA seems to become more accurate than the TFM, even at the highest k considered, but with perhaps an excess of variance transfer at very high k for $Pr = 0.0625$. We shall soon speculate as to why this should be so.

We focus next on the TFM results in figure 2. For the scalar transfer, the

agreement with DNS is better in the range $0.25 \leqslant Pr \leqslant 2.0$, becoming poorer for Pr outside this range, especially for $T_\theta(k)$ as $Pr \to 0$. Overall, for all values of Pr investigated, the excess DNS energy in the dissipation range, as compared to that for the TFM, may signal the presence of small-scale intermittency in the former and absence of it in the latter. In this connection, Métais & Lesieur (1991) have found flatness factors for $\partial_x \theta$ of ≈ 5 for $Pr = 1$, which indicates significant intermittency for the scalar derivatives and for the $\Theta(k)$ spectrum at high k. On the other hand, at large Pr (≈ 8), $E_\theta(k)$ for DNS exceeds that of the TFM by a factor of about 2, and this may be a result of 'inertial range' (i.e. large-scale) intermittency. However, considering the better performance of the DIA in the energy-containing range for large Pr, we cannot rule out that the 'Markovian' aspects of the TFM render it unable to follow with accuracy rapidly decaying turbulence, such as the case here.

The DIA (shown in figure 2 by the dashed lines) compares favourably to the TFM at the smaller Pr, but not so well at large Pr, especially in the dissipation range. As mentioned above, its poor behaviour at $Pr > 1$ may be understood in terms of its spurious sensitivity to large-scale sweeping (lack of invariance to random Galilean transformations (Kraichnan 1964)). Thus instead of $E_\theta(k) \sim \epsilon_\theta (\nu/\epsilon_u)^{\frac{1}{2}} k^{-1}$ as the high Pr, Batchelor *et al.* (1959) inertial range, the DIA has $E_\theta(k) \sim E_0^{\frac{1}{2}} \epsilon_\theta / (\nu/\epsilon_u)$, *independent of* k. In these expressions, ϵ denotes dissipation of the indexed quantity, and E_0 is the total kinetic energy. Although such an analysis is usually made for large Reynolds numbers, reflections on its derivation suggest that it applies to small R_λ as well, at least for sufficiently large Pr.

The errors in TFM at $Pr = 0.0625$ may be thought surprising (see especially figure 2*f*), since we expected progressively weakened non-Gaussian effects as $Pr \to 0$, at least according to Batchelor *et al.* (1959). We note that the TFM incorporates this low-Pr theory of BHT in quantitative form: as $Pr \to 0$, TFM $\Rightarrow$ BHT.

The discrepancy at low k between TFM and DNS for $Pr = 0.0625$ may be attributable to sample errors. There are after all only two wavenumber bins where $T_\theta(k) \leqslant 0$. But sampling errors at larger k (where $T_\theta \geqslant 0$) are small, and the TFM underestimation of T_θ is significant. The extent of the DNS–TFM discrepancy may be judged by comparing DNS and the TFM for the mixed scalar skewness, (2.5). For $Pr = 1/16$ this is (0.286, 0.177) for DNS and the TFM respectively. On the other, the DIA gives $S_{uu\theta} = 0.260$.

The comparisons of the DNS, DIA, and TFM discussed here suggest that the reason the TFM gives increasingly poor results as $Pr \to 0$ is associated with the fact that Markovian closures (such as the TFM) underestimate energy (or scalar variance) transport, when compared to their non-Markovian counterpart. Generally, a Markovianization of a theory weakens transport to small scales, by scrambling (through its representation of the turbulent force $(\boldsymbol{u} \cdot \boldsymbol{\nabla} \boldsymbol{u})$ as white noise) features which would otherwise be aligned with the dominant strain. As noted by Herring & Kerr (1982), such an underestimation increases rapidly as $R_\lambda \to 0$ (see their figure 8). According to that study, the TFM begins to severely underestimate the velocity derivative skewness, S_{uuu} for $R_\lambda \leqslant 5$. On the other hand, the DIA (which is not Markovianized) compares well with DNS, down to the lowest $R_\lambda \approx 0.5$ investigated.

The scalar equivalent of R_λ is the (microscale) Péclet number,

$$P_\lambda \equiv \{\langle u^2 \rangle \langle \theta^2 \rangle / \langle \partial\theta/\partial x)^2 \rangle\}^{\frac{1}{2}} / (Pr\nu).$$

By analogy with the remarks of the last paragraph, we may expect the Markovianization errors to become significant for $P_\lambda \lesssim 5$. For the present study, and for $Pr = 0.25$, P_λ is 6.59, whereas for $Pr = 0.0625$, $P_\lambda = 3.03$. The low-Pr discrepancy

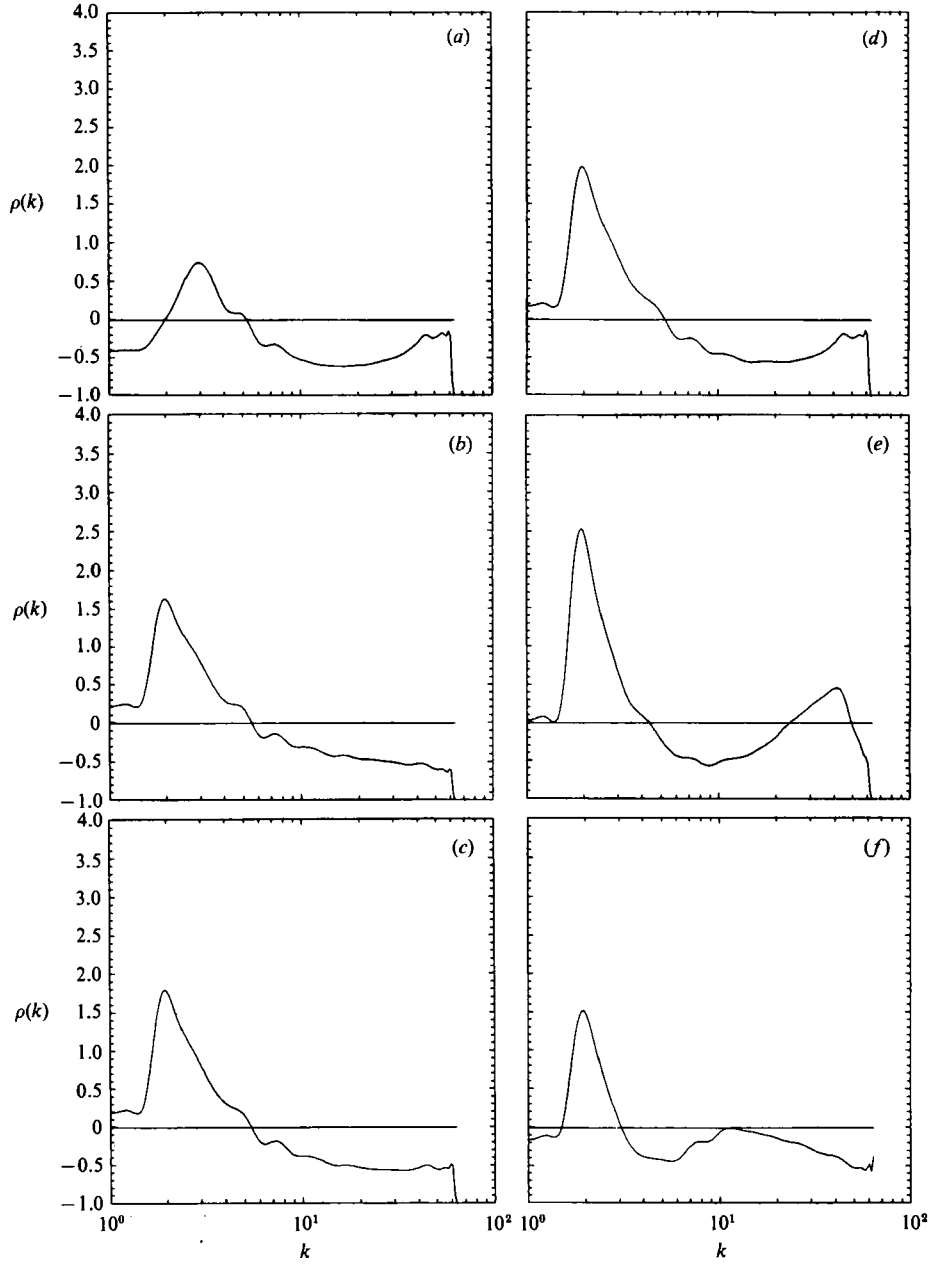

FIGURE 3. $\rho(k,t) \equiv F_\theta(k)/F_\theta^G(k) - 1$, a measure of the non-Gaussianity of the 'nonlinear' force, given by (3.15). Here $F_\theta^G(k)$ is the value of $F_\theta(k)$ if the fields $\boldsymbol{u}(\boldsymbol{k},t), \theta(\boldsymbol{k},t)$ were Gaussian (see (3.13)–(3.14)).

discussed here relates to the variance transfer function, whereas the TFM–DNS comparison for $E_\theta(k,t)$ (as shown in figure 1*f*) is more satisfactory, at least for the time span investigated.

We next give some information on non-Gaussian aspects of the scalar transfer mechanism by examining the statistics of the 'forcing function' in the equations of motion for $\theta(\boldsymbol{k},t)$. That is, writing (2.6) in the form

$$(\partial_t + \kappa k^2)\,\theta(\boldsymbol{k},t) = f_\theta(\boldsymbol{k},t), \tag{3.13}$$

we ask for those statistical descriptors of $f_\theta(\boldsymbol{k}, \boldsymbol{u}, \theta)$ that indicate non-Gaussian behaviour. The simplest of these is the variance spectra of $f_\theta(\boldsymbol{k})$,

$$F_\theta(k,t) \equiv \langle |f_\theta(\boldsymbol{k})|^2 \rangle. \tag{3.14}$$

We compare F_θ to what would be obtained if $(\boldsymbol{u}(\boldsymbol{k}), \theta(\boldsymbol{k}))$ were from a multivariate Gaussian distribution using the spectrum

$$\rho(k,t) \equiv -1 + F_\theta(k)/F_\theta^{\mathrm{G}}(k) \tag{3.15}$$

as a simple measure of non-Gaussianity. Note that (3.15) defines $\rho(k)$ to be the ratio of correlated power to the Gaussian. Here, F_θ^{G} is that F obtained for $(\boldsymbol{u}(\boldsymbol{k}), \theta(\boldsymbol{k}))$ multivariate Gaussian, with the same spectra $E_u(k)$, $E_\theta(k)$ and $(\langle \boldsymbol{u}(\boldsymbol{k})\,\theta(-\boldsymbol{k}) \rangle = 0)$ as the evolved fields. Comparisons are given in figure 3(*a–f*), with figure 3(*a*) the ratio for the velocity force spectra. A comparison of figures 2 and 3 shows that ρ reaches a maximum for wavenumbers exceeding those of maximum energy extraction, where $T_{u,\theta}(k)$ is strongly negative. At higher k, where $T_{u,\theta} > 0, \rho(k)$ becomes negative and remains so until the far dissipation-range scales. These scales are larger than the aliasing wavenumber $k_{\mathrm{a}} = 42$. The negative region defines scales for which the flow's structures have small 'Eulerian' accelerations. The magnitude of $\rho \sim 0.5$ is typical of the reduction of the 'turbulence force' observed in other simulations, and is also predicted by statistical theories (Herring 1980*b*; Kraichnan & Panda 1988; Chen *et al.* 1989).

With respect to the kinetic energy transfer we are in agreement with the statements of Domaradzki & Rogallo (1990), who note good agreement between DNA and EDQNM for moderate R_λ. However, their study was for a spectrum $E(k,0) \sim k(k_0+k)\exp(-ck)$ which is centred much more on large scales than (3.11), and hence decays more slowly with less vigorous transfer. These authors, moreover, normalize their EDQNM estimates with those of their DNS, thereby testing only the shape of the energy transfer function at a single time.

4. Bispectra results

To facilitate the DNS evaluation of (1.1) and (2.1), we use the equivalence between ensemble and space averaging to write the physical space form of the bispectra as

$$B_{uuu}(x_1, x_2) \equiv \left(\frac{1}{2L}\right)^3 \int_{-L}^{L} \mathrm{d}x \int_{-L}^{L} \mathrm{d}y \int_{-L}^{L} \mathrm{d}z\, u(\boldsymbol{x})\, u(\boldsymbol{x} + \iota x_1)\, u(\boldsymbol{x} + \iota x_2). \tag{4.1}$$

Here $2L$ is the periodic box size, assumed large compared to integral scales of the turbulence, and ι is the unit vector in the direction of u. The discretized version of (4.1) (as implemented by (2.4)) is used to compute the DNS version of B_{uuu} and $B_{\theta\theta u}$. For isotropic initial conditions, statistical scatter in (4.1) may be reduced by using coordinate labelling equivalences.

DNS results for $B_{uuu}(x_1, x_2)$ and $B_{\theta\theta u}(x_1, x_2)$ are presented in figure 4(*a*, *b*). Here initial conditions are

$$E_{u,\theta}(k,0) = Ck^8 \exp(-4(k/k_0)^2) \tag{4.2}$$

with $C \ni \int_0^\infty \mathrm{d}k E(k) = 1$, $k_0 = 8$, and $\nu = \kappa = 0.01$. Initial conditions in (4.2) evolve more rapidly than those studied in §3, and additionally allow the large scales (small k) to develop according to dynamics rather than to be fossils of the initial conditions. Since the spectra are centred at higher k than (3.11), they also have smaller statistical

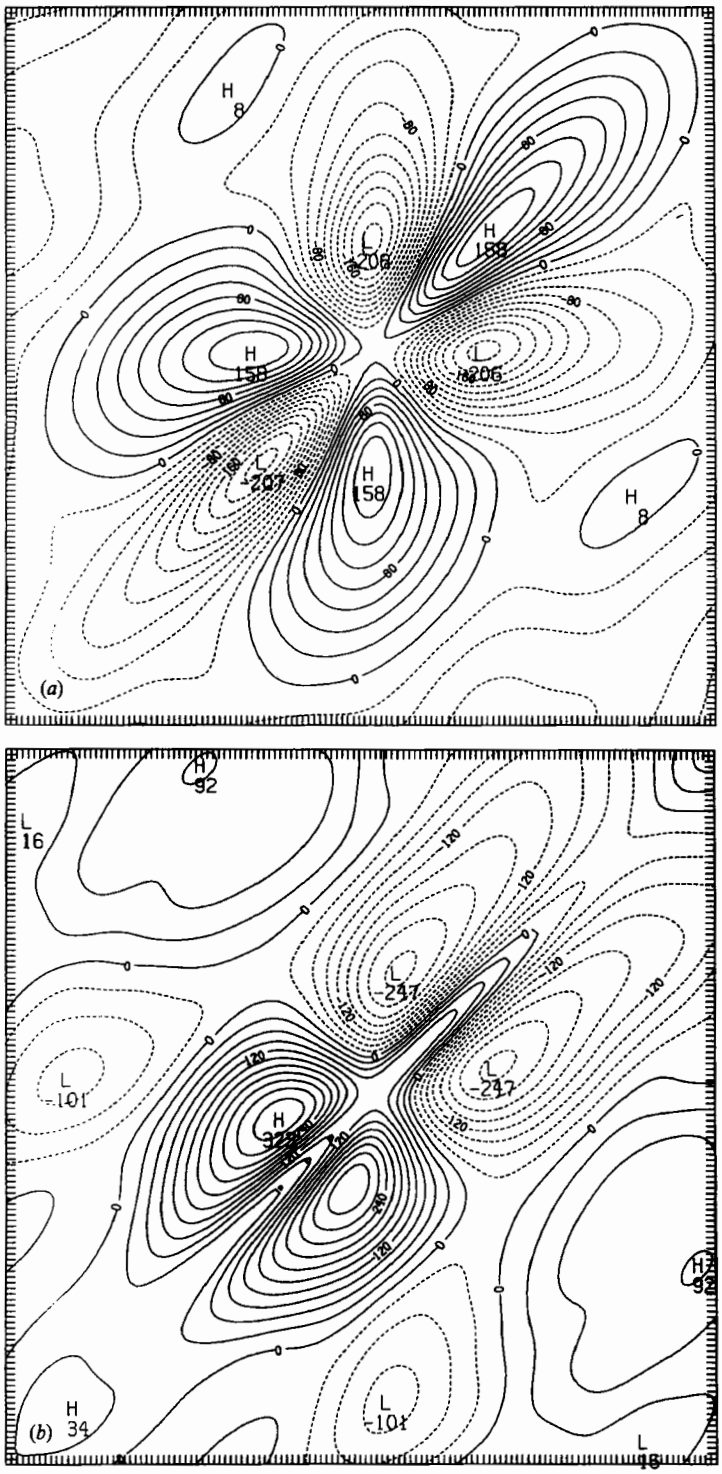

FIGURE 4. (a) DNS $B_{uuu}(x_1, x_2)$, and (b) $B_{\theta\theta u}(x_1, x_2)$, for decaying turbulence whose initial spectrum is (4.2). Resolution of DNS is 128^3. The evolution time is $t = 1.233$.

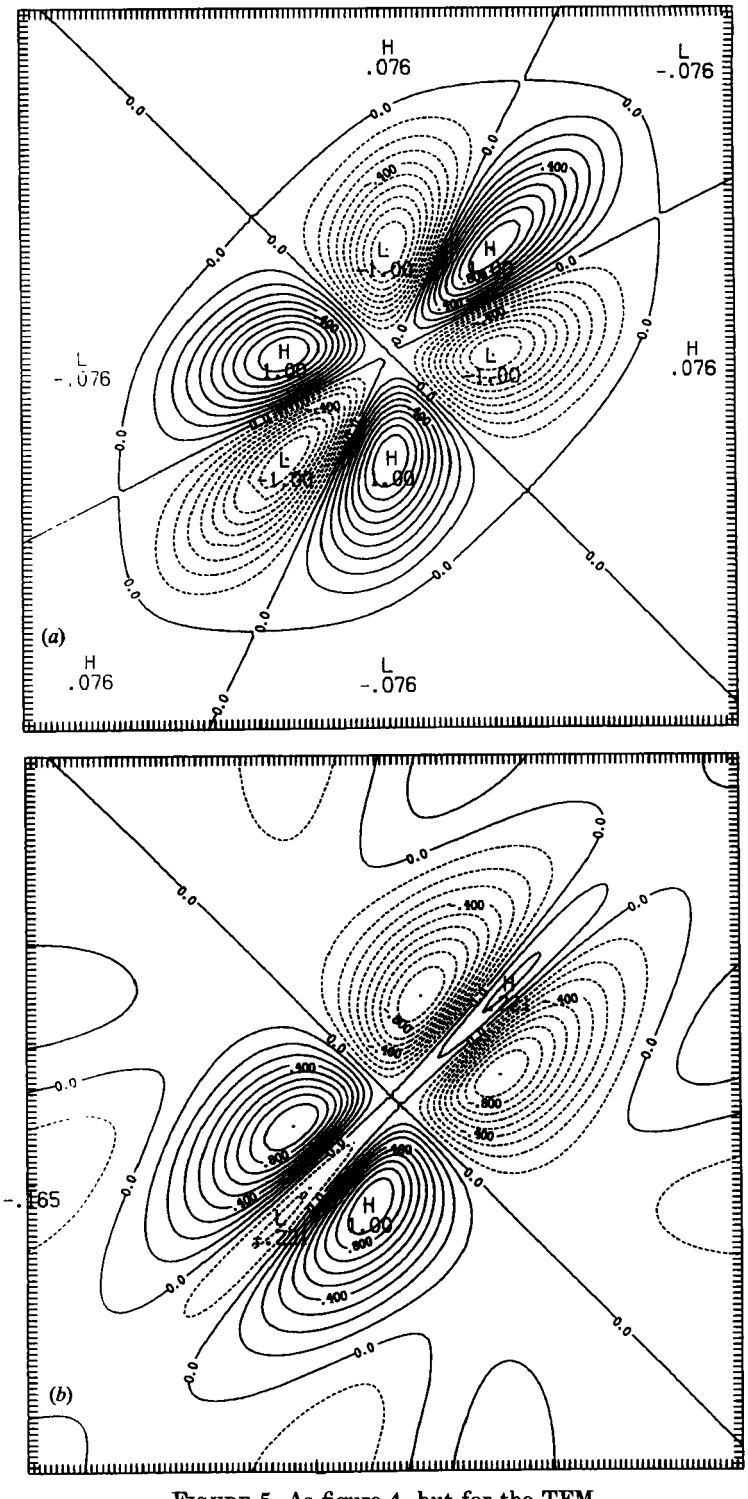

FIGURE 5. As figure 4, but for the TFM.

scatter, attributable to the finite band averaging (3.12). The price paid for lower scatter is a lowering of R_λ: for (3.11 a, b), at the time for which the spectra of figures 1 and 2 are shown ($t = 1.00$), $R_\lambda \sim 20$, while for (4.2) (at $t = 1.22$, the time at which bispectra are displayed), $R_\lambda \sim 10$. Spectra (4.2) were used in the DNS study of Lesieur & Rogallo (1989), and the comparative DNS–TFM study of Herring (1990). However, in those studies the viscosity and conductivity were replaced by turbulent viscosity and conductivity, which allows much higher effective R_λ to be examined.

In discussing figure 4(a, b) it is useful to have the integral scale

$$L_u \equiv \left(\frac{3\pi}{4}\right)\int_0^\infty k^{-1}E(k)\,\mathrm{d}k/\int_0^\infty E(k)\,\mathrm{d}k,$$

and Taylor microscale

$$\lambda_u \equiv [\langle u^2\rangle/\langle(\partial_x u)^2\rangle]^{\frac{1}{2}}.$$

These are 0.4017, and 0.2623, while the equivalent scalar lengthscales

$$L_\theta \equiv \left(\frac{\pi}{2}\right)\int_0^\infty k^{-1}E_\theta(k)\,\mathrm{d}k/\int_0^\infty E_\theta(k)\,\mathrm{d}k, \quad \lambda_\theta = [\langle\theta^2\rangle/\langle(\partial_x\theta)^2\rangle]^{\frac{1}{2}}$$

are 0.2885, 0.1817). Thus, the width of the major leaf along the 45° axis (as measured by the zero-contour) is $\sim 0.63L_u$, and the width of the positive lobe in the third quadrant of figure 4(b) is $\sim 0.40L_\theta$.

The symmetry $x_1 \to x_2$ is apparent in figure 4(a, b) as is the higher symmetry of B_{uuu} relative to that of $B_{\theta\theta u}$. Of course, much of the busy small-scale features at large $|x_1 - x_2|$, result from the finite size of the discrete representation of the averages in (4.1). On the other hand, it seems clear that the six-leaf rose at the centre of figure 4(a), and the five-leaf rose of figure 4(b) are real features. These central features of the DNS are also a property of the TFM bispectra as well. The TFM results are shown in figure 5(a, b). The maximum in B_{uuu} occurs at a distance of 1.22 from the origin, which is about $1.1L$, where L is the integral scale of the turbulence.

Along $x_1 = x_2$, we expect positive values of B for ($x_1, x_2 \geqslant 0$), (and negative for (x_1, x_2) $\leqslant 0$). For B_{uuu}, this follows from simple advection arguments for u^2, and for $B_{\theta\theta u}$ the same argument for θ^2 holds (recall that $B_{\zeta\zeta u}(x_1, x_1) = \langle\zeta^2(x_1)\,u(0)\rangle$). This positive region for $x_1 \geqslant 0$ should persist for about one large-scale correlation length along the diagonal. Transverse to the diagonal, the advective correlation region is shorter, particularly for $B_{\theta\theta u}$. Notice that in figure 4(b) for $B_{\theta\theta u}$ no negative region is discernable along $x_1 = x_2, x_1 \leqslant 0$. This violation of an antisymmetry feature, we believe, is attributable to the accidental asymmetry in the initial data of the DNS. As noted in the introduction, the violation of symmetry (1.4) stems from a lack of (statistical) reflectional invariance of the initial data for DNS. For the velocity field, a measure of the violation of (1.2) is the normalized helicity,

$$\langle \boldsymbol{u}\cdot\boldsymbol{\nabla}\times\boldsymbol{u}\rangle/(\langle u^2\rangle^{\frac{1}{2}}(\langle(\boldsymbol{\nabla}\times\boldsymbol{u})^2\rangle^{\frac{1}{2}}),$$

which for the DNS considered here has an initial value of 0.0182. The corresponding measure for θ would be

$$\int \mathrm{d}\boldsymbol{k}\,\langle\theta_{\mathrm{r}}(\boldsymbol{k})\theta_{\mathrm{i}}(\boldsymbol{k}\rangle/\int \mathrm{d}\boldsymbol{k}\langle|\theta(\boldsymbol{k})|^2\rangle,$$

but we have no data on this point. (Subscripts r and i denote real and imaginary parts.)

Figures 6 and 7 compare the DNS and TFM for $B'_{uuu} \equiv \mathrm{i}k_1k_2(k_1+k_2)B_{uuu}(k_1, k_2)$ and $B'_{\theta\theta u} \equiv \mathrm{i}k_1k_2(k_1+k_2)B_{\theta\theta u}(k_1, k_2)$. Here, multiplication by the factor $\mathrm{i}k_1k_2(k_1+k_2)$

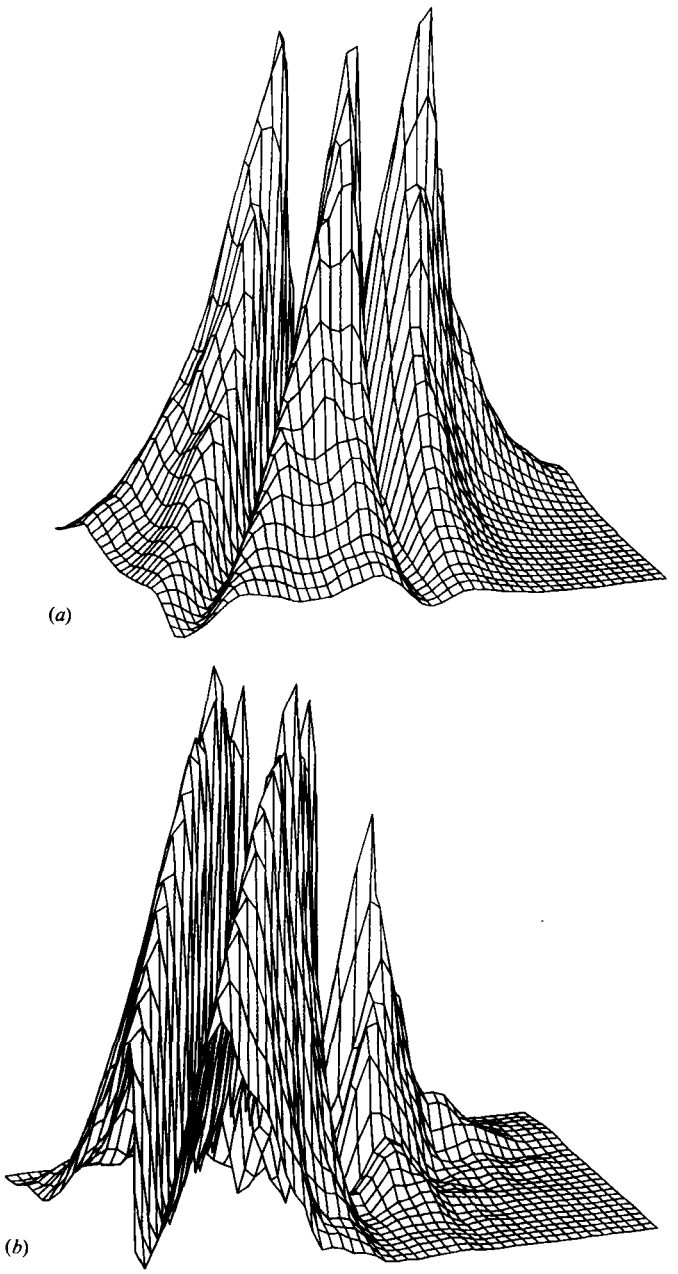

FIGURE 6. Fourier-transformed derivative bispectra: (*a*) $B'_{uuu}(k_1, k_2) \equiv \mathrm{i}k_1 k_2(k_1+k_2)B_{uuu}(k_1, k_2)$, and (*b*) $B'_{\theta\theta u}(k_1, k_2) \equiv \mathrm{i}k_1 k_2(k_1+k_2)B_{\theta\theta u}(k_1, k_2)$ for DNS. Initial conditions are (4.2), and evolved time is $t = 1.23$ large-scale eddy turnover times.

means that the B' are the bispectra of derivatives of the fields comprising the B. As noted in the introduction, and in the discussion surrounding (2.5),

$$\int_{-\infty}^{\infty} \mathrm{d}k_1 \int_{-\infty}^{\infty} \mathrm{d}k_2 B'$$

is proportional to the corresponding derivative skewness. Figure 7 shows the half-

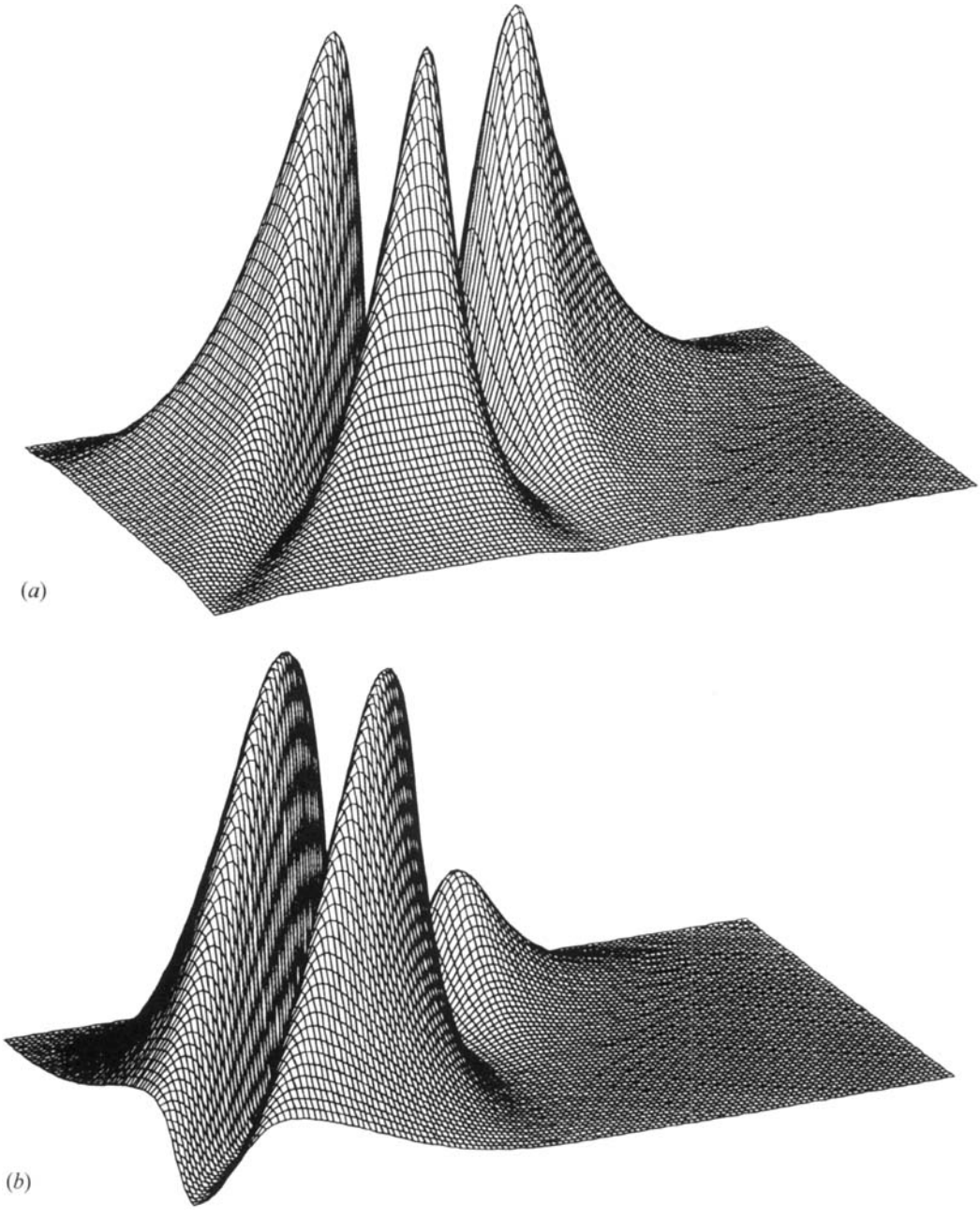

FIGURE 7. As figure 6 but for the TFM.

plane, $(-k_{\max} \leqslant k_2 \leqslant k_{\max})$, $(0 \leqslant k_1 \leqslant k_{\max})$, $k_{\max} = 64$. For $B'_{uuu}(k_1, k_2)$, the definitional symmetry (1.1) implies $B'_{uuu}(k_1, k_2) = B'_{uuu}(k_2, k_1) = B'_{uuu}(k_1, -k_1 - k_2)$. For $B'_{\theta\theta u}$, the second symmetry is absent. Thus, as is evident in figure 6, the negative quadrant of B'_{uuu} is implied by the positive quadrant, but such is not so for $B'_{\theta\theta u}$. It is of interest to note that for the skewness S'_{uuu}, two-thirds of its contribution comes from the negative quadrant (and its complex counterpart), while for $S'_{\theta\theta u}$, the dominance of the negative quadrant is even stronger.

5. Discussion and concluding remarks

We have examined here nonlinear aspects of energy and scalar variance decay from two separate perspectives. The first, traditional to turbulence theory, consists of comparing theory and simulation for the spectral transfer function $T_{u,\theta}(k,t)$ for a range of Prandtl numbers ($0.0625 \leqslant Pr \leqslant 8.0$). Here, for $R_\lambda \sim 30$, we note a reasonable agreement between the TFM and DNS for large Pr, but a perhaps surprising lack of agreement for $Pr \leqslant 0.25$. Again, we recall that the discrepancy described here pertains to the variance transfer function at small scales; the DNS–TFM comparison for the variance spectrum (as shown in figure 1*f*) is more satisfactory.

These findings concur with earlier DNS results of Kerr (1985), who noted that at low Pr, $S_{\theta\theta u}$ from DNS was significantly larger than that estimated from the low-Pr BHT theory. Basically, this theory is an assertion (for scalar-velocity cumulants) of *single time* quasi-normality in the limit $Pr \to 0$, and is coincident with the TFM in this limit. We have also compared the DNS to the DIA, and this comparison suggests that the low-Pr (TFM–DNS) discrepancy stems from the 'Markovian' step in the derivation of the TFM. The DIA, on the other hand, becomes equivalent to a two-time quasi-normal scalar variance theory as $Pr \to 0$. This statement holds only with respect to the scalar field. The low-Pr agreement of the DIA with DNS is better than that of the TFM; it is not perfect, as illustrated by the significant excess transfer at high k for $Pr = 0.0625$. There are presumably some effects here of the lack of random Galilean invariance; it would be of interest to consider the Lagrangian history theory (Kraichnan 1964), or the Lagrangian theory of Kaneda (1981), to see if either performs better in this regard.

We have argued that the small-scale variance transfer errors in the TFM become serious as $Pr \to 0$ when the microscale Péclet number drops below about 5. Our reasoning here is by analogy with the velocity field dynamics, and is as yet unsupported by computations at high R_λ and low Pr. The basic point is that Markovianization weakens transfer to small scales. Perhaps the clearest illustration of this point is the early decay calculations of Herring & Kraichnan (1972), who note a $\sim 30\%$ decrease in the velocity derivative skewness in passing from the DIA to its Markovian version (essentially Edward's 1964 theory). In any case, we would not argue that such errors are serious for sufficiently high R_λ at any Pr.

Chasnov (1991) has recently reported good agreement between large-eddy simulations and BHT in the inertial-conductive range for both decaying and forced stationary turbulence. However, we should note that the discrepancy addressed in the present paper pertains in large part to the dissipation range, where the mixed scalar skewness receives most of its contribution. This region is not assessable in Chasnov's simulation, since the large-eddy simulations have no realistic dissipation range.

Gibson (1968) (see also Gibson, Ashurst & Kerstein 1988) has suggested that the failure of the BHT theory to maintain a sufficiently large value of $S_{\theta\theta u}$ with decreasing Pr is associated with the accumulation of scalar fluctuations in the neutral point of the flow, in such a way that $S_{\theta\theta u}$ depends dominantly on the small-scale strain (for any Pr). This hypothesis would imply that the small-scale structures are unexpectedly immune to molecular dissipation. Generally, we expect the presence of such structures to be manifested by a non-Gaussian distribution function for θ. In this connection, our examination of the 'scalar force' (equation (3.14)) for a range of Pr suggested only moderate non-Gaussianity at the higher range of Pr, and

increasing Gaussianity with decreasing Pr). Such findings do not lend support to Gibson's ideas, but clearly numerical results at sufficiently large R_λ so that the 'Markovian' problem is not encountered are needed in order to be conclusive.

An additional comment with respect to the DIA comparison is that it seems superior to the TFM in the energy-containing range at all Pr investigated. This may signify its ability to capture more faithfully the rapidly evolving dynamics of low R_λ flow than a 'Markovian' theory such as the TFM.

The second perspective, that of the bispectra, is perhaps more directly related to measurements, but less revealing of dynamics. Thus, B_{uuu} comprises elementary triple-moment correlations, but not in a way directly related to the energy transfer function, $T(k,t)$. Bispectra have the same relationship to energy transfer as one-dimensional spectra have to the three-dimensional spectra: both tend to smooth out any small-scale details.

We should note, however, that in a certain respect, bispectra discriminate between velocity and scalar transfer mechanisms better than the energy transfer. Thus in figure 2(*a*), $T_u(k)$ is qualitatively indistinguishable from figure 2(*d*) ($T_\theta(k)$, $Pr = 1$), whereas the distinction between figure 4(*a*), $B_{uuu}(x_1, x_2)$, and figure 4(*b*), $B_{\theta\theta u}(x_1, x_2)$, is clear. Of course the dimension of B is 2, whereas that of T is 1.

The TFM bispectra comparisons clearly reproduce the topological features of both B_{uuu}, and $B_{\theta\theta u}$ (see figures 4 and 5). Moreover, the comparisons of derivative bispectra for DNS and TFM in figure 6 are also in reasonable accord. To make a quantitative assessment of these comparisons complete, we must face the question of statistical scatter produced by the finite nature of the DNS, and the dependency of the results on the random numbers used to initialize fields $\boldsymbol{u}$ and θ. One approach to this problem is to compare DNS bispectra from (4.1) with equivalent results averaging over only the $x-y$ directions, i.e. including only the $(x-y)$ sums in (4.1) as implemented by (2.4). Such comparisons (not shown here) indicate this reduced symmetry averaging $(x-y)$ to be entirely adequate to give even quantitative features of $B_{uuu}, B_{\theta\theta u}$.

Part of this research was done while J. R. H. was Professeur Associé à l'Institut de Mécanique de Grenoble. Both authors are grateful to Professor M. Lesieur of INPG for many useful discussions. We also are grateful to Dr O. Thual, of the Advanced Study Program of NCAR (and CERFACS, Toulouse, France) for consultations and assistance in implementing the FFT's used in bispectra evaluation. We also benefited from several discussions with R. M. Kerr and R. H. Kraichnan. Some of the calculations reported here were carried out at the Centre de Calcul Vectoriel pour la Recherche Palaiseau, France.

REFERENCES

Batchelor, G. K., Howells, I. D. & Townsend, A. 1959 Small-scale variation of convected quantities like temperature in turbulent fluid. Part 2. The case of large conductivity. *J. Fluid Mech.* **5**, 134–139.

Betchov, R. 1957 An inequality concerning the production of vorticity in isotropic turbulence. *J. Fluid Mech.* **1**, 497–504.

Chasnov, J. 1991 Simulation of the inertial-conductive subrange. *Phys. Fluids* **3**, 1164–1168.

Chasnov, J., Canuto, V. M. & Rogallo, R. S. 1988 Turbulence spectrum of a passive temperature field: results of a numerical simulation. *Phys. Fluids* **31**, 2065–2067.

Chen, H. D., Herring, J. R., Kerr, R. M. & Kraichnan, R. H. 1989 Non-Gaussian statistics in isotropic turbulence. *Phys. Fluids* A **1**, 1844–1854.

DANNEVIK, W. P., YAKHOT, V. & ORSZAG, S. A. 1987 Analytical theories of turbulence and the ϵ-expansion. *Phys. Fluids* **30**, 2021–2029.

DOMARADZKI, J. A. & ROGALLO, R. S. 1990 Local energy transfer and nonlocal interactions in homogeneous, isotropic turbulence. *Phys. Fluids* A **2**, 413–426.

EDWARDS, S. F. 1964 The theoretical dynamics of homogeneous turbulence. *J. Fluid Mech.* **18**, 239–273.

GIBSON, C. H. 1968 Fine structure of scalar fields mixed by turbulence. I. Zero-gradient points and minimal gradient surfaces. *Phys. Fluids* **11**, 2305–2315.

GIBSON, C. H., ASHURST, W. T. & KERSTEIN, A. R. 1988 Mixing of strongly diffusive passive scalars like temperature by turbulence. *J. Fluid Mech.* **194**, 261–293.

HERRING, J. R. 1980*a* Theoretical calculations of turbulent bispectra. *J. Fluid Mech.* **97**, 193–204.

HERRING, J. R. 1980*b* A note on Owens' mesoscale eddy simulation. *J. Phys. Oceanogr.* **10**, 804–806.

HERRING, J. R. 1990 Comparison of closure to spectral-based large eddy simulations. *Phys. Fluids* A **2**, 979–983.

HERRING, J. R. & KERR, R. M. 1982 Comparison of direct numerical simulations with predictions of two-point closures for isotropic turbulence convecting a passive scalar. *J. Fluid Mech.* **118**, 205–219.

HERRING, J. R. & KRAICHNAN, R. H. 1972 Comparison of some approximations for isotropic turbulence. *Models and Turbulence* (ed. M. Rosenblatt & C. Van Atta). Lecture Notes in Physics, vol. 12, pp. 148–194. Springer.

HERRING, J. R., SCHERTZER, D., LESIEUR, M., NEWMAN, G. R., CHOLLET, J. P. & LARCHÊVEQUE, M. 1982 A comparative assessment of spectral closure as applied to passive scalar diffusion. *J. Fluid Mech.* **124**, 411–437.

KANEDA, Y. 1981 Renormalized expansions in the theory of turbulence with the use of the Lagrangian position function. *J. Fluid Mech.* **107**, 131–145.

KERR, R. M. 1985 Higher-order derivative correlations and the alignment of small-scale structures in isotropic numerical turbulence. *J. Fluid Mech.* **153**, 31–58.

KRAICHNAN, R. H. 1959 The structure of isotropic turbulence at very high Reynolds numbers. *J. Fluid Mech.* **5**, 497–543.

KRAICHNAN, R. H. 1964 Lagrangian-history closure approximation for turbulence. *Phys. Fluids* **8**, 575–598.

KRAICHNAN, R. H. 1971 An almost-Markovian Galilean-invariant turbulence model. *J. Fluid Mech.* **47**, 513–524.

KRAICHNAN, R. H. & PANDA, B. 1988 Depression of nonlinearity in decaying isotropic turbulence. *Phys. Fluids* **31**, 2395–2397.

LARCHEVÊQUE, M., CHOLLET, J. P., HERRING, J. R., LESIEUR, M., NEWMAN, G. R. & SCHERTZER, D. 1980 Two-point closure applied to a passive scalar in isotropic turbulence. In *Turbulent Shear Flows 2*, pp. 50–66. Springer.

LARCHEVÊQUE, M. & LESIEUR, M. 1981 The application of eddy-damped Markovian closure to the problem of dispersion of particle pairs. *J. Méc.* **20**, 113–134.

LESIEUR, M., MÉTAIS, O. & ROGALLO, R. 1989 Étude de la diffusion turbulente par simulation des grandes échelles: *C. R. Acad. Sci. Paris* **308** (II), 1395–1400.

LESIEUR, M. & ROGALLO, R. 1989 Large-eddy simulation of passive scalar diffusion in isotropic turbulence. *Phys. Fluids* A **1**, 718–722.

MÉTAIS, O. & LESIEUR, M. 1991 Spectral large-eddy simulation of isotropic and stably stratified turbulence. *J. Fluid Mech.*

NEWMAN, G. R. & HERRING, J. R. 1979 A test field model of a passive scalar in isotropic turbulence. *J. Fluid Mech.* **94**, 163–194.

VAN ATTA, C. W. 1979 Inertial range bispectra in turbulence. *Phys. Fluids* **22**, 1440–1442.